Characterization of Zeolite L Nanoclusters

Michael Tsapatsis,*,†,‡ Mark Lovallo,‡ Tatsuya Okubo,†,§ Mark E. Davis,*,† and Masayoshi Sadakata§

Chemical Engineering, California Institute of Technology, Pasadena, California 91125, Department of Chemical Engineering, University of Massachusetts, Amherst, Massachusetts 01003, and Department of Chemical System Engineering, The University of Tokyo, 7-3-1 Hongo, Bonkyo-ku, Tokyo 113, Japan

Received May 11, 1995. Revised Manuscript Received June 30, 1995®

Zeolite L (structure code LTL) crystals are synthesized starting from homogeneous potassium aluminosilicate solutions. Particle size and shape of the formed zeolite L are examined by high-resolution transmission electron microscopy, field emission-scanning electron microscopy, X-ray diffraction, and dynamic light scattering. The synthesis conditions reported lead to nanoclusters of aligned zeolite crystalline domains of dimensions ~40 nm in the channel direction and ~15 nm in the direction perpendicular to the zeolite channels. The nanoclusters have sizes of ~60 nm. Electron microscopy of the nanoclusters reveals the presence of inhomogeneities (intercrystalline porosity) on length scales ranging from 2 to 60 nm. The N_2 and cyclohexane adsorption capacities and the thermal stability of the crystals synthesized are correlated with their microstructure. The preparation of colloidal suspensions of the zeolite L nanoclusters in water is described along with their use in seeded growth and film formation.

Introduction

Control of the shape and size of zeolite crystals is desirable for particular applications. In the traditional utilization of zeolites as catalysts, adsorbents, and ion exchangers, the crystal size can affect the performance (apparent activity, selectivity, rates of adsorption) by influencing the characteristic diffusion time through the crystallite.[1,2] Additionally, subtle, more indirect effects of crystal size and morphology have been speculated to occur.[3] For example, in addition to the short diffusion path, the more uniform distribution of aluminum in small ZSM-5 crystallites was shown to have an effect on *p*-xylene selectivity in toluene methylation and disproportionation.[3] Influence of the particle shape on the activity of zeolite L on aromatization of acyclic hydrocarbons has also been reported.[4]

In addition to the catalytic applications of zeolite ultrafine (nanocrystalline) particles, our interest in their synthesis stems from their potential use as precursors for thin-film formation through sol-gel processing of colloidal suspensions.[5] Due to the small size of the nanoparticles they are particularly well suited for the formation of stable colloidal suspensions. The preparation of colloidal suspensions of zeolite particles with particle sizes of about 100 nm has been reported for sodalite and zeolites A, Y, and ZSM-5.[6-8] Recently, Meng et al.[9] reported the synthesis of zeolite L particles with crystal sizes as low as 20 nm as determined by X-ray diffraction (XRD) line-broadening (analyzed using the Scherrer equation). Various syntheses were described, and the conditions were optimized for product purity and minimal crystal size. However, the details of the crystal morphology were not investigated. Ultrafine zeolite L has been described in the patent literature by Vaughan et al.[10] These investigators have reported the preparation of nanocrystalline zeolite L with sizes as small as 10 × 15 nm by reacting potassium aluminosilicate gels with aqueous ammonia solvents. These crystallites are reported to be in an agglomerated state. In another patent, the preparation of similarly sized zeolite L crystals is claimed.[4] By transmission electron microscopy (TEM) the crystallites are observed to be aligned in the agglomerates within ±15°.[4]

The detailed morphology of the crystallites and stage of agglomeration are of paramount importance for thin-film processing since it influences the stability and rheological properties of the suspensions. Moreover, from this standpoint, to achieve minimal film thickness and interzeolitic porosity, the zeolite and agglomerate size and size distribution width should be minimized.

Zeolite L possesses a one-dimensional large pore system parallel to the *c* axis of the crystal. The unit cell has hexagonal symmetry (*P*/6*mmm*) with $a = 1.84$

† California Institute of Technology.
‡ University of Massachusetts.
§ The University of Tokyo.
* Corresponding authors.
® Abstract published in *Advance ACS Abstracts,* August 1, 1995.

(1) Fajula, F. In *Guidelines for Mastering the Properties of Molecular Sieves*; Barthoneuf, D., Derouane, E. G., Hölderich, W., Eds.; Nato ASI Series; Plenum Press: New York, 1989; p 53.
(2) Rajagopalan, K.; Peters, A. W.; Edwards. G. C. *Appl. Catal.* **1986**, *23*, 69.
(3) Shiralkar, V. P.; Joshi, P. M.; Eapen, M. J.; Rao, B. S. *Zeolites* **1991**, *11*, 511.
(4) Verduijn, P. V.; Mechilium, J.; De Gruijter, C. B.; Koetsier, W. T.; Van Oorschot, C. W. M. U.S. Patent, 5,064,630, 1991.
(5) Tsapatsis, M.; Okubo, T.; Lovallo, M.; Davis, M. E. In *Advances in Porous Materials*; Komarnemi, S., Smith, D. M., Beck, J. S., Eds.; MRS: Vol. 371, 1995.
(6) Schoeman, B. J.; Sterte, J.; Otterstedt, J. E. *Zeolites* **1994**, *14*, 208.
(7) Schoeman, B. J.; Sterte, J.; Otterstedt, J. E. *Zeolites* **1994**, *14*, 110.
(8) Persson, A. E.; Schoeman, B. J.; Sterte, J.; Otterstedt, J. E. *Zeolites* **1994**, *14*, 557.
(9) Meng, X.; Zhang, Y.; Meng, C.; Pang, W. In *Proceedings of the 9th International Zeolite Conference,* Montreal 1992; von Ballmoos, R., et al., Eds.; Butterworth-Heinemann: London, 1993; p 297.
(10) Vaughan, D. E. W.; Strohmaier, K. G. Canadian Patent Application, 2,106,170, 1994.

0897-4756/95/2807-1734$09.00/0

nm and c = 0.75 nm.[11] The minimum constricting aperture is defined by a ring of 12 tetrahedral atoms (T atoms, e.g., Si, Al) that forms an opening of 0.71 nm. The most often observed shape of zeolite L crystals is cylindrical with the channels running parallel to the central axis of the cylinder while several modifications of shape have been reported through synthetic modifications.[12]

High-resolution transmission electron microscopy (HRTEM) has been used to study the grain boundaries and stacking faults in zeolite L crystallites.[13] A stacking fault is the coincidence boundary ($\sqrt{13}.\sqrt{13}$ R 32.2° superstructure) and was first reported by Terasaki et al.[14] De Gruyter et al. have identified 0° and 30° tilt boundaries as well as 30° twist boundaries.[15] These authors have used the information on the grain boundaries of zeolite L to deduce information on the growth events that take place during crystallization.

To relate electron microscopy results with particle morphology, it is necessary to verify that drying and sample preparation do not alter the crystallite characteristics. Moreover, since electron microscopy probes a small portion of the sample, the statistical validity of the results should be confirmed. Dynamic light scattering (DLS) has been used to provide statistically valid direct measurements of crystal growth events of zeolites A, Y, and ZSM-5 and hydroxysodalite.[6,7] Electron microscopy and DLS measurements complement one another in providing a picture of the particle characteristics. Comparison of direct DLS measurements with the electron micrographs provides a valuable consistency test that can be used to help clarify ambiguities introduced by sample preparation for TEM.

In this report we characterize zeolite L nanoclusters by XRD, DLS, field emission scanning electron microscopy (FE-SEM), and HRTEM. We show that different aspects of the morphology are probed by the various techniques. Additionally, we characterize the nanoclusters with respect to their thermal and adsorption properties. Moreover, we show that stable colloidal suspensions of zeolite L nanoclusters in water can be prepared.

Experimental Section

Materials. Aluminum foil (0.05 mm thick, 99.8+%, Aldrich) and fumed silica (Grade M-5, Cabosil) were used to prepare aluminate solutions and silicate solutions, respectively. The alkali-metal ion source was potassium hydroxide (A.C.S grade, Fisher).

Synthesis and Product Recovery. A clear potassium aluminate solution was prepared by the addition of 3.6 g of aluminum foil to 150 mL of a 3 M aqueous KOH solution. The solution was filtered to remove the iron impurities of the aluminum foil that remained undissolved.

Fumed silica (80 g) was dissolved in 300 mL of 3 M KOH solution with stirring and heating at 80 °C for 12 h. After cooling to room temperature, slow addition of the clear aluminate solution to the clear silicate solution with vigorous stirring resulted in a clear homogeneous solution. Subsequent adjustments of the concentrations were performed with the addition of water or aqueous KOH. Preweighed amounts of the synthesis solution were placed in Teflon-lined, stainless-steel pressure vessels and were heated in a forced convection oven with rotation (rotating speed ~30 rpm). The resulting solids were recovered by centrifugation (centrifugal force 40 000 g for 2 h). The solid samples were repeatedly washed (centrifuged and redispersed in water using ultrasonication) until the pH of the dispersion was below 8. This washing process was necessary to increase the stability of the zeolite in the electron microscope when performing high-resolution studies. TEM results showed that sonication had no major effect on the crystallite shape. Solid yields were calculated by weighing the solids obtained after drying at 110 °C for 12 h.

Characterization. Dynamic light scattering was used to determine the average particle size and particle size distribution using an ELS-800 (Otsuka Electronics) spectrometer equipped with a 10 mW He–Ne laser. The detector was fixed at 90° angle with respect to incident beam direction. Number-weighted data and standard deviations are reported as determined by the instrument. Number-averaged values allow for comparison with electron microscopy results. For DLS the sample preparation was as follows: 0.06 mL of the suspension being examined was diluted with 2.94 mL of KOH aqueous solution having the same pH of the suspension or with 2.94 mL of H_2O. In some cases the samples were sonicated before the measurement.

For transmission electron microscopy, a drop of the zeolite suspension in water was transferred to a carbon-coated Cu grid. The grid was allowed to dry at 110 °C and was mounted on a single-tilt specimen holder. Micrographs were recorded using a Phillips 430 microscope operated at 200 kV and a JEOL 100 CX or JEOL 2000 FX microscope operating at 100 and 200 kV, respectively. EDAX was performed in the STEM mode to obtain the Si/Al ratio of the samples with an electron spot size of ~10 nm. Bulk elemental analyses were performed using inductively coupled plasma spectroscopy (ICP).

Scanning electron micrographs were recorded using a Hitachi S-900 FE-SEM. The specimens were coated with Pt for a few seconds using an ion sputter system equipped with a magnetron electrode (Hitachi E-1030).

XRD patterns were collected on a Scintag XDS-2000 diffractometer equipped with a liquid nitrogen-cooled germanium detector using Cu Kα radiation. Data were taken with a step size of 0.03° and with a step time of 6 s. For crystalite size determination by XRD line broadening, the Scherrer equation was used: $l = K\lambda/((B^2 - \beta^2)^{1/2}\cos(2\theta/2))$ where l is the average crystalite size, K = 0.893, λ = 0.15405 nm, B is the peak broadening of the (221) peak of the sample in radians, and β is the instrumental peak broadening in radians determined using lanthanum hexaboride (NIST standard reference material 660). Temperature-programmed X-ray diffraction (TPXRD) was performed using a heated stage in an environmental chamber. For a limited number of samples, the XRD data were collected at the National Synchrotron Light Source in Brookhaven National Laboratory. The sample was placed in a 1 mm capillary. A 10 mm × 16 mm beam of 1.30042 Å was used with a Si (111) single-reflection incident beam monochromator. The sample was scanned with a 0.05° step and 8 s count time between steps.

Nitrogen adsorption isotherms were collected at 77 K using an Omicron 100 analyzer. Cyclohexane adsorption was performed on a McBain-Bakr balance at room temperature with pressures up to P/P_o = 0.5. The samples were activated by heating at 250 °C under vacuum.

Differential thermal analysis (DTA) was performed (DuPont Instruments 910) using a heating rate of 5 °C/min in air and with α-Al_2O_3 as reference.

Results and Discussion

Growth Curves. The crystallization process was followed as a function of heating time for a synthesis starting from a clear solution with molar composition $10K_2O-1Al_2O_3-20SiO_2-400H_2O$. The yield of solids in

(11) Meier, W. M.; Olson, D. H. *Atlas of Zeolite Structure Types*; Butterworth: London, 1987; p 88.
(12) Wortel, T. M. US Patent, 4,544,539, 1985.
(13) Treacy, M. M. J.; Newsam, J. M. *Ultramicroscopy* 1987, *23*, 411.
(14) Terasaki, O.; Thomas, J. M.; Ramdas, S. *J. Chem. Soc., Chem. Commun.* **1984**, 216.
(15) De Gruyter, C. B.; Verduijn, J. P.; Koo, J. Y.; Rice, S. B.; Treacy, M. M. J. *Ultramicroscopy* **1990**, *34*, 102.

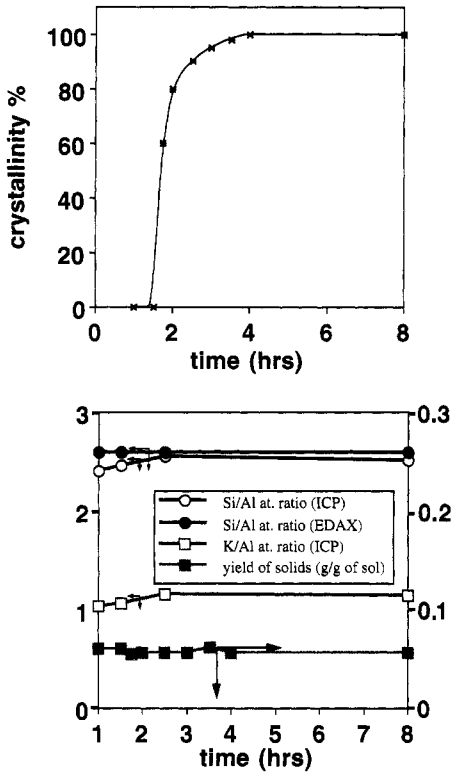

Figure 1. Yield and composition of solid products and growth curve of zeolite L for crystallization at 175 °C starting from a clear solution with composition $10K_2O-1Al_2O_3-20SiO_2-400H_2O$.

grams per gram of solution, the percent crystallinity from XRD, and the Si/Al and K/Al ratios as determined by ICP and EDAX are given in Figure 1 for various crystallization times at 175 °C. The percent crystallinity is estimated here as the ratio of the intensity of the (221) peak of the solid samples at various times of crystallization to the intensity of the (221) peak of the solid sample crystallized for 8 h.

The growth curves and visual observation during synthesis show that although the crystallizing mixture starts as a clear homogeneous solution, an amorphous (as determined from XRD, electron microscopy, and electron diffraction) gelatinous precursor is formed early in the crystallization process. The gel gradually collapses to a suspension as crystallization proceeds. The complete disappearance of the gel coincides with 100% crystallinity of zeolite L. The ultimate yield of zeolite is 0.055 ± 0.005 g/g of sol and reaches this value at 4 h of heating. An interesting observation is that the total yield of solid products remains constant for all heating times greater than 1 h even though the crystallinity increases from 0 to 100% between 1 and 4 h of heating. Moreover, the Si/Al ratio of the solid products obtained after 1 h of heating (as determined by EDAX analysis on the STEM) is found to be constant and equal to ~2.6. By analyzing several locations of the sample at a resolution of ~10 nm, it was confirmed that Al is distributed "uniformly" throughout the samples. Bulk analysis (ICP) shows a constant Si/Al ratio from the amorphous gel to the fully crystalline solid. The K/Al ratio is not measured by EDAX since such measurements are unreliable due to beam damage.[13] The values estimated by bulk chemical analysis (ICP) show a constant K/Al ratio of ~1 in the product throughout gelation and crystallization.

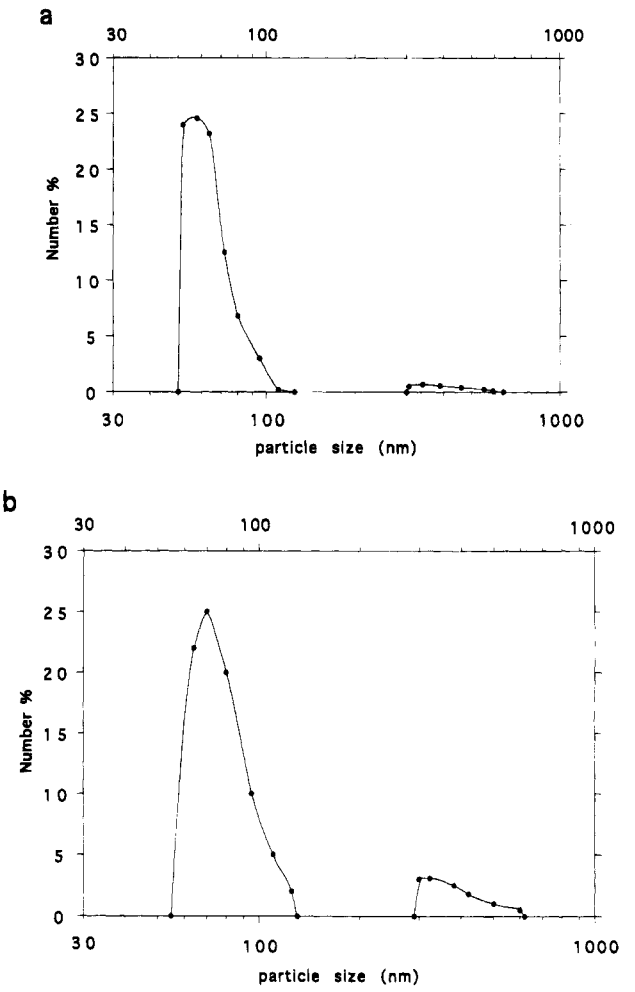

Figure 2. Stokes diameter distributions determined by DLS for the zeolite suspensions in their mother liquid for (a) 4 h and (b) 12 h of crystallization (synthesis conditions as described in Figure 1).

These observations along with HRTEM observations of solids from early stages of crystallization are discussed elsewhere[16] with respect to the mechanism of zeolite formation. The growth curve presented here suggests that a gel with Si/Al and K/Al ratios close to that of the zeolite product is formed upon heating. We believe that the gel formation is followed by a rapid transformation of the gel to zeolite without changes in the yield of solids and the Al/Si/K ratio. Evidently, the gel-to-suspension transformation is caused by the reduction of solid volume due to the higher density of the zeolite crystals as compared to the density of the amorphous gel. The crystalline particles remain in suspension because of their small size and the high concentration of electrolyte (KOH and soluble silicate species).

Dynamic Light-Scattering Measurements. Initial analyses were performed on zeolite suspensions in their mother liquid. Considerable variation of the DLS results from measurement to measurement and the curve shape of the autocorrelation function indicated a polydisperse system. Figure 2 shows the Stokes diameter distributions (averages from 15 measurements of each sample) as determined by analyzing samples in their mother liquid after dilution with H_2O. For heating

(16) Tsapatsis, M.; Davis, M. E., submitted.

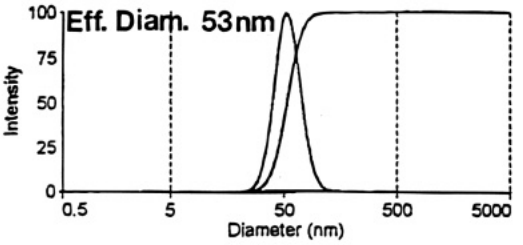

Figure 3. Stokes diameter distributions determined by DLS for the zeolite suspension in water (pH ~7).

times shorter than 4 h there remains some millimeter-sized gel fragments that prevent meaningful analysis of DLS results. After 4 h of heating, the crystallization reaches completion (100% crystallinity by XRD) and the number-averaged particle size is estimated by DLS to be ~60 nm. A small number of larger particles is present (on a weight basis this small number represents a substantial part of the zeolite mass). Further heating does not induce significant changes in the particle size. After 12 h of heating, the particle size is increased to ~80 nm with the small number of larger particles (~400 nm) still present.

Analysis of the washed samples (dispersion of zeolite L in water at pH ~7) gave a nearly monodispersed size distribution (polydispersity ~0.1) as shown in Figure 3. The determined average Stokes diameter is somehow smaller (~50 nm) and there is no evidence of larger particles. The small shift in the Stokes diameter of the smaller population from 60 to 50 nm upon washing of the samples probably reflects changes in diffusivities due to differences in the ionic strength of the liquid rather than an actual particle size reduction. On the other hand, the disappearance of the indication of larger particles at the washed samples is interpreted as loose aggregate breakage during washing, centrifugation, and redispersion by sonication. The formation of loose aggregates by association of the 60 nm population in the mother liquid can be understood if we consider its higher pH and ionic strength. This view is supported by DLS measurements in the mother liquid after sonication. Measurements performed immediately after sonication give no evidence of the 400 nm population. Within minutes after sonication the larger size population gradually reappears.

From the DLS data it can be concluded that a nearly monodisperse population of zeolite L particles is produced with average Stokes diameter ~60 nm with an indication of a minor population of larger aggregates. Due to the irregular, elongated, shape of the particles, as evidenced by the electron microscopy studies described below, the Stokes diameter can be used only as an approximate estimation of particle size.

Transmission and Scanning Electron Microscopy. Figures 4 and 5 show TEM and SEM micrographs of the zeolite particles obtained after 7 h of heating.

TEM. The TEM photograph shows numerous nearly cylindrical zeolite domains that have approximate dimensions of ~15 nm in diameter and less than 50 nm in length. These domains form larger clusters with dimensions comparable to those determined by DLS measurements (~60 nm). Some degree of bonding of the domains within a cluster is suggested from their alignment and the fact that sonication and washing fail

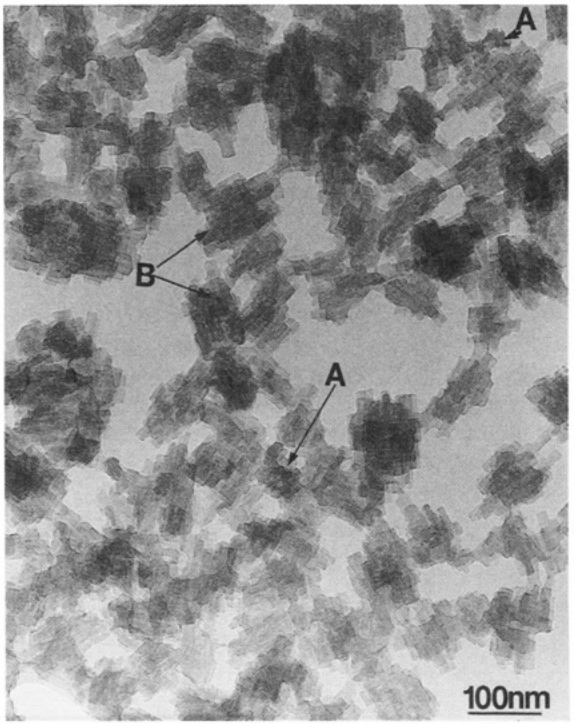

Figure 4. TEM of zeolite L after 7 h of heating (other synthesis conditions as described in Figure 1). Particles marked A are oriented with their *c* axis nearly parallel to the electron beam. Particles marked B are oriented with their *c* axis nearly perpendicular to the electron beam.

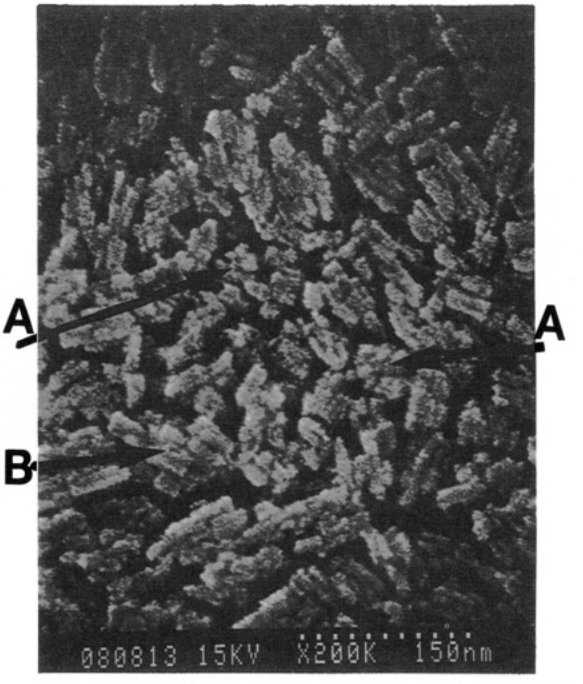

Figure 5. FE–SEM of zeolite L after 7 h of heating (other synthesis conditions as described in Figure 1). Particles marked A are oriented with their *c* axis nearly parallel to the electron beam. Particles marked B are oriented with their *c* axis nearly perpendicular to the electron beam.

to break the clusters into smaller particles. The agreement in the estimated particle size between TEM and DLS confirms that the agglomeration process does not take place during the washing and drying of the samples. No evidence of the 400 nm particles is found in the electron micrographs. This strengthen the view expressed above that their presence is associated with

aggregation in the mother liquid of the 60 nm clusters to form loose aggregates that can be broken upon sonication. In the micrograph, shown in Figure 4 most of the clusters are arranged on the Cu grid with their *c* axis (channel direction) perpendicular to the electron beam. Less often clusters were found with their *c* axis parallel to the electron beam, allowing a view down the zeolite channels. Some isolated nanocrystals are also evident in the photographs. No major quantifiable change of the particle morphology is observed for crystallization times between 4 and 12 h at 175 °C from analysis of numerous photographs.

FE–SEM. TEM provides 2-D projections of the 3-D particles; therefore TEM images like that shown in Figure 4 cannot be used to readily assess the density of the clusters. On the other hand SEM micrographs as shown in Figure 5 provide a 3-D perspective of the particles at a lower resolution and are complementary to TEM observations. The discrete nanocrystalline domains forming the clusters are evident in the SEM micrograph. Considerable porosity exists in each cluster formed by the void spaces between the nanocrystalline domains. The clusters have a nearly dentritic appearance with "fjords" having a length scale of the order of the cluster size. The TEM micrographs give the false impression of the clusters being dense due to overlapping of the projections of the nanocrystalline domains.

HRTEM. HRTEM images are shown in Figure 6. Figure 6a shows a view down the *c* axis of a small isolated crystallite of nanoscale dimensions. Such isolated crystals are often observed but constitute only a small fraction of the sample (<5%). The 12-member rings are clearly resolved in this image, and higher resolution information is also present as evidenced by the digital diffractogram. The three peripheral domains marked A, B, and C show a higher contrast than the intermediate region, suggesting a different thickness along the crystal.

HRTEM micrographs of typical zeolite L clusters are shown in Figures 6b,c. The crystalline domains are aligned with their *c* axis nearly parallel to one another within a cluster. This allows the observation of the 12 T-atom channels in views down [001] as in Figure 6b. Numerous small angle or 0° tilt boundaries are evident. Digital diffractograms of numerous such clusters show a 6-fold symmetry with the characteristic spacing of zeolite L. 30° rotational boundaries[14,15] are not observed.

In Figure 6c the alignment is shown more clearly. Fringes corresponding to (001) planes are resolved and are shown to be aligned throughout the cluster.

In view of the observation that the clusters consist of aligned domains of nanoscale dimensions, we refer to them as nanoclusters. The FE-SEM and HRTEM images show that the zeolite L nanoclusters have inhomogeneities ranging from ~20 Å (HRTEM observations) to the size of the nanoclusters, ~60 nm (SEM observations).

XRD. Line-broadening calculations using the Scherrer equation were performed on the XRD patterns. Analysis based on the (221) peak broadening gave results in agreement with those reported by Meng et al.[9] for samples examined from various crystallization times: particle size of ~20 nm with no changes between 2 and 12 h of heating. In view of the morphology of the

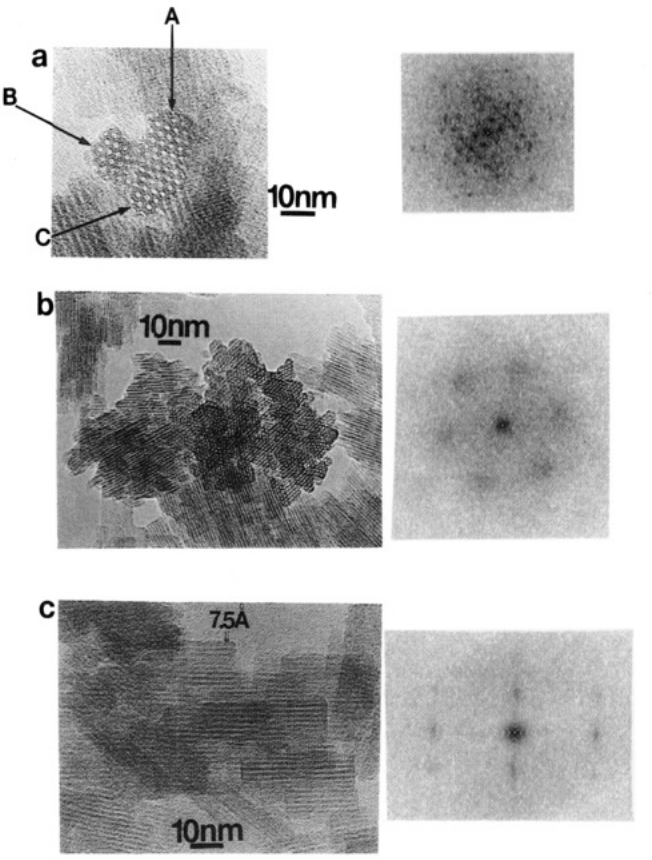

Figure 6. (a) HRTEM of zeolite L nanocrystal synthesized after heating for 7 h (other synthesis conditions as described for Figure 1) and corresponding digital diffractogram. Such isolated nanocrystals constitute a small fraction of the sample. (b) HRTEM of zeolite L nanocluster oriented with the *c* axis parallel to the electron beam and corresponding digital diffractogram. (c) HRTEM of zeolite L nanocluster oriented with the *c* axis perpendicular to the electron beam and corresponding digital diffractogram.

nanoclusters as shown by electron microscopy, it is evident that XRD line broadening probes the size of the domain and not of the nanoclusters. This is expected due to the discontinuities (porosity) of the nanoclusters.

Synchrotron XRD data from zeolite L nanoclusters prepared after 9 h of heating were used to investigate further details of the morphology of the nanocrystalline domains. Analysis of the (001) peak gave an estimation of a particle size of ~40 nm while the (220) peak broadening corresponds to 15 nm. Additionally the (221) peak broadening gives an estimation of the size that is in agreement with the conventional XRD analysis presented above (~20 nm). The anisotropic broadening suggests that the domains are prismatic with the prism "height" (indicated by the (001) peak broadening) greater than its "diameter" (indicated by the (220) peak broadening). These values are volume averages of the domain size and thus tend to underestimate the contribution of much finer domains observable in the TEM micrographs.

Midsynthesis Addition of Aluminum. Zeolite L is known to crystallize at a fixed Si/Al ratio of 3. Using a Si/Al ratio of 3, a 0.055 g/g of solution yield corresponds to ~80% consumption of the Al initially present in the crystallizing solution. Similarly, yields of Si and K show that ~25% of the Si and 30% of the K were consumed during the crystallization. These calculations

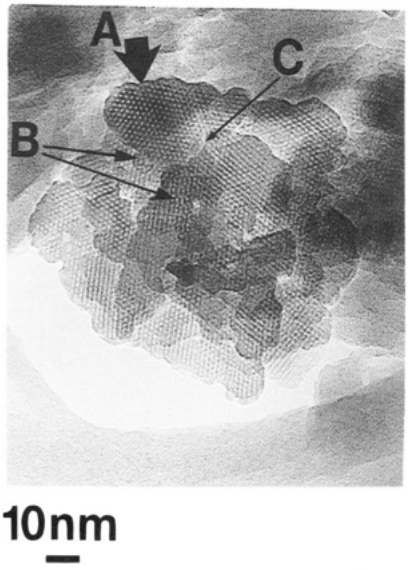

Figure 7. HRTEM image of zeolite L formed after midsynthesis addition of Al (synthesis conditions as described in the text). The view is down the *c* axis. Grain marked A is rotated by 30° to the rest of the cluster. B: 30° rotational boundary. C: 30° tilt boundary.

suggest that aluminum is the limiting reactant. Midsynthesis addition of Al was employed to observe whether crystal growth could be continued. A similar experiment involving the midsynthesis addition of Al has led to an increased size of hydroxysodalite.[6] An aluminate solution (10 mL) of composition $3.5KOH-1.6Al_2O_3-200H_2O$ was added to 40 mL of the primary synthesis solution after 7 h of crystallization. The new combined solution was further heated at the original reaction conditions for another 8 h. Samples were collected and prepared in the same manner as described previously.

Recovery of the solid sample showed an increase in yield from the original value of 0.055 to 0.11 g/g of sol. This increased yield is due to secondary growth of particles existing in the solution after 7 h of crystallization and/or to nucleation of new crystallites (or amorphous material) during the final 8 h of crystallization.

Figure 7 shows a HRTEM micrograph of a zeolite L cluster after midsynthesis addition of aluminate solution. A comparison of this micrograph with that of the primary crystallized particles (Figure 6b) reveals that the overall size and shape of the nanocluster has not significantly changed but the domain size has increased. These results indicate that the majority of the secondary crystallization occurs within the voids between the nanosized crystallites formed during primary crystallization. This phenomenon can be more clearly observed in micrographs that contain clusters oriented with the electron beam down the *c* axis as in Figure 7. The agglomerates are more dense and are comprised of larger crystallites. Also, the view in this direction reveals the existence of 30° twist boundaries that were not observed in agglomerates from primary crystallization. This defect shows that a certain degree of nucleation takes place after midsynthesis addition of Al.

Line broadening calculations from the (221) peak using the Scherrer equation give an estimate of 30 nm for the domain size as compared to 20 nm for crystallites before midsynthesis addition in agreement with the TEM observations.

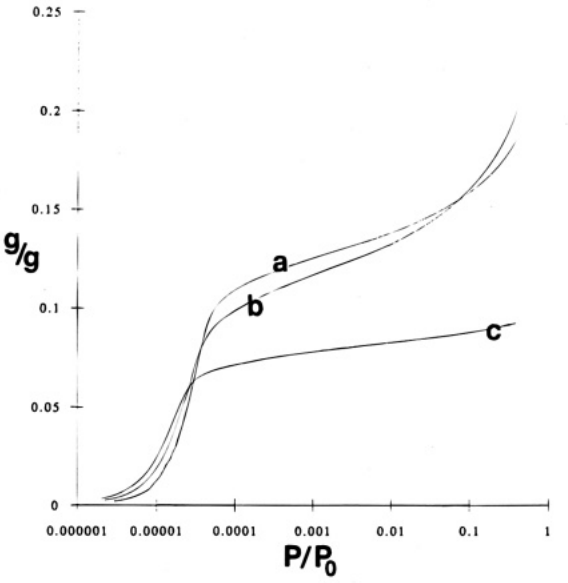

Figure 8. Nitrogen adsorption at 77 K of (a) zeolite L formed with midsynthesis addition of Al; (b) zeolite L before midsynthesis of Al; (c) micron-sized zeolite L.

Nitrogen and Cyclohexane Adsorption and DTA Results. Figure 8 shows the nitrogen adsorption isotherms for the crystallites synthesized with and without midsynthesis addition of Al along with the isotherm for micron-sized crystals. The adsorption results are consistent with the results presented above suggesting the presence of inhomogeneities in the micro- and mesoscopic scales. In the pressure region where microporous adsorption occurs, the nanoclusters exhibit a greater adsorption capacity compared with the micron-sized crystals, indicating the presence of additional microporosity between the nanocrystalline domains. At higher pressures the presence of mesoporosity accounts for the observed differences.

Cyclohexane adsorption experiments also are consistent with the TEM results. A greater capacity for adsorption (0.19 mL/g at $P/P_0 = 0.5$) is observed for the nanoclusters from primary crystallization than for the ones grown with midsynthesis addition of Al (0.14 mL/g). The presence of 30° twist boundaries as well as the higher density of the clusters after midsynthesis addition of Al should be the cause of this effect. The cyclohexane adsorption capacity of micron-sized crystallites ranges from 0.10 to 0.12 mL/g.

DTA results are shown in Figure 9 and provide information on the thermal stability of the zeolite L nanoclusters. Zeolite L from the primary growth is stable up to temperatures around 950 °C. The zeolite L formed after midsynthesis addition of aluminum shows a somewhat greater stability to temperatures up to 1000 °C evidently due to the larger domain size. Larger, micron-sized, crystals of zeolite L were found to be stable up to 1100 °C. TPXRD results are consistent with the DTA results. Thus, the nanocrystals are less stable than micron-sized zeolite L. However, the differences are not large.

Preparation of Colloidal Suspensions. The resulting suspensions of zeolite L nanoclusters in their mother liquid start settling when stored at room temperature, and a layer of clear liquid is observed after 2 days. This is unlike the colloidal suspensions of ZSM-5 and sodalite which have been reported to be stable for

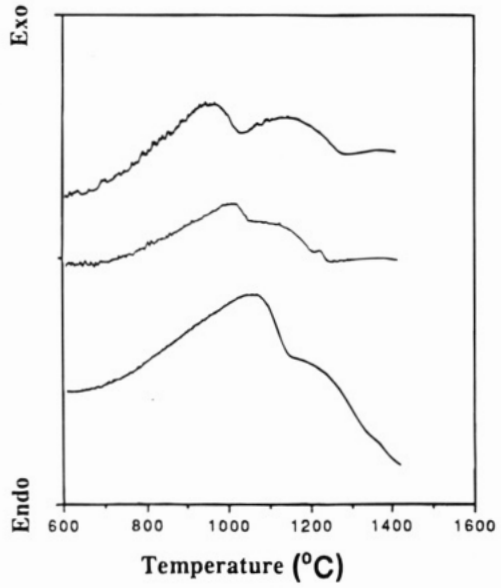

Figure 9. DTA results for (top) zeolite L formed before midsynthesis addition of Al; (middle) zeolite L formed with midsynthesis addition of Al; (bottom) micron-sized crystals of zeolite L.

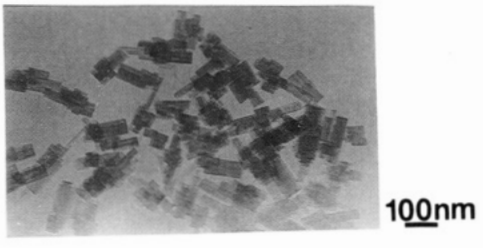

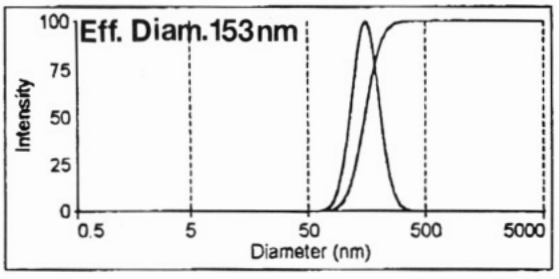

Figure 10. TEM image and Stokes diameter distribution determined by DLS of the zeolite L crystals produced from seeded growth in a solution with composition $10K_2O-1Al_2O_3-20SiO_2-2000H_2O$ (175 °C for 6 h).

months in their mother liquid.[7] The DLS results presented above provide evidence that aggregation of the nanoclusters takes place in the mother liquid. However, stable suspensions of zeolite L nanoclusters can be prepared with repeated washing, centrifugation, and redispersion in water by sonication. Suspensions of the zeolite L clusters in water (pH ~7) with concentration of ~20 g/L do not show any change in particle size (as determined by DLS) for at least up to 3 months (~60 nm). These suspensions can be used for the preparation of crack free transparent films.[5]

Use of the Colloidal Suspensions for Seeded Growth. For the purposes of film formation[5] and size tailoring of zeolite L crystals, identification of conditions that lead to controlled growth of the nanocrystals is needed. We have performed experiments where weighted amounts of the colloidal suspensions were added to a

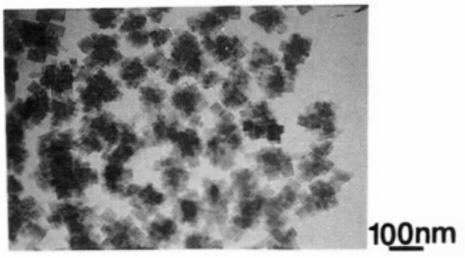

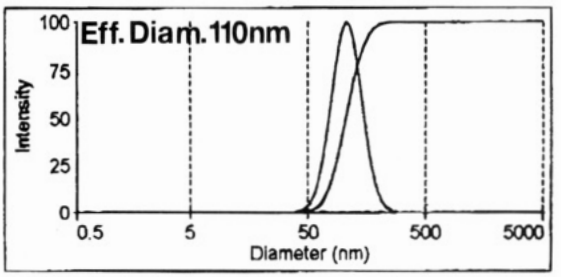

Figure 11. TEM image and Stokes diameter distribution determined by DLS of the zeolite L crystals produced from seeded growth in a solution with composition $10K_2O-1Al_2O_3-20SiO_2-1200H_2O$ (175 °C for 6 h).

Figure 12. FE-SEM top view of zeolite L film prepared from a nanocluster suspension after evaporation of the water.

homogeneous solution, resulting in liquid compositions which do not nucleate zeolite L. An example of such an experiment which leads to growth of the zeolite particles is described below.

A zeolite suspension (10 g/L) in water (pH ~7) was added to a homogeneous, potassium aluminosilicate solution resulting in a solution with composition $10K_2O-1Al_2O_3-20SiO_2-2000H_2O$ with 5.5 g/L nanocluster seeds. A synthesis starting from a clear solution with this composition (no zeolite L added) results in an amorphous product when heated for up to 8 h at 175 °C. With the zeolite nanoclusters present, no amorphous precipitate is formed, and the crystals grow larger to almost perfect cylinders after 6 h as shown in Figure 10. The zeolite nanoclusters due to their high surface

area can serve as seeds for growth without further nucleation. By varying solution compositions, seeded growth can result in different morphologies. Figure 11 shows morphologies of regrown crystals in a solution with composition $10K_2O-1Al_2O_3-20SiO_2-800H_2O$ (175 °C for 6 h). This composition, without addition of zeolite L nanocluster seeds results in micron-sized zeolite L crystals. It is thus demonstrated that a certain control on the growth of the seeds can be achieved. This is of importance for the formation of compact zeolite L films.

Film Formation. The zeolite L nanocluster suspensions were used for the preparation of unsupported films by evaporation of the water in a petri dish placed in a desiccator. The films are microcrack free and transparent. A FE-SEM micrograph is given in Figure 12. The films are very fragile since the zeolite L clusters are not bonded together. However, their mechanical strength can be increased with the addition of a binder such as alumina or silica. The preparation and characterization of these composite films will be described elsewhere.

Conclusions

We have shown that a combination of XRD, DLS, FE-SEM, and TEM provides information on different aspects of morphology and gives a detailed picture of the structure of zeolite L nanoclusters. The zeolite L nanoclusters consist of aligned, nearly prismatic, nanometer scale domains (15 × 40 nm) and have an elongated shape and size. The Stokes diameter is ~60 nm. It is also shown that stable colloidal suspensions of the zeolite L nanoclusters in water can be prepared (at pH ~7) free of any organic or inorganic additives. Finally, conditions have been identified for controlled growth of the zeolite L nanoclusters to larger and more compact crystallites.

Acknowledgment. Funding for this work was provided by ARCO. Acknowledgment is made to the donors of the Petroleum Research Fund, administered by the American Chemical Society, for partial support of this research. The authors would like to thank Mrs. Carole Garland for valuable assistance in the TEM, Dr. R. Lobo and Dr. J. Higgins for the acquisition of the synchrotron data, and Prof. S. Suib and Brookhaven Instruments Corp. for providing access to their experimental facilities. The synchrotron XRD data were collected at X7A beam line, National Synchrotron Light Source, Brookhaven National Laboratory, which is supported by the Department of Energy, Division of Materials Science and Division of Chemical Sciences.

CM9502129